Title: Performance evaluation of portable Dual-Spot micro-aethalometers for source identification of Black Carbon aerosols from Wildfire Smoke and Traffic Emission in the Pacific Northwest.

Mrinmoy Chakraborty, Amanda Giang, Naomi Zimmerman

Section A: Abbreviations and notations used in this study

eBC	Equivalent black carbon concentration. Aethalometer reported black carbon.
MAC	Mass Absorption Cross section
BC	Black Carbon
ATN_1, ATN_2	Light attenuation measured in aethalometer from the photometer readings at filter spot 1 and filter spot 2
PM2.5	Particles with size up to 2.5 μm
I_0, I_1 , I_2	Light intensity measured by photometer from reference spot, aerosol loaded spot 1 and aerosol loaded spot 2 respectively
$b_{abs,\lambda}$	Light Absorption Coefficient at wavelength λ nm
$b_{abs,NC}$	Non-corrected b_{abs} derived from MA300 raw photometer data
$b_{abs,D}$	Drinovec-corrected b_{abs} derived from MA300 raw photometer data
α	Ångström exponent
α_{ff}	Constrained value of Ångström exponent for fossil fuel-based aerosol
α_{bb}	Constrained value of Ångström exponent for biomass burning based aerosol
C	Scattering correction factor
ξ	Lateral leakage factor on the aethalometer filter
k	Loading correction factor
A	Area of loaded filter spot on aethalometer
F_1 , F_2	Aerosol laden air flow rate on filter spot 1 and filter spot 2
MA300 eBC	eBC reported by MA300 units which uses onboard correction scheme
MA300 b_{abs}	b_{abs} derived from MA300 reported data which uses onboard correction scheme
eBC_{bb}	Apportioned eBC component from biomass burning based sources
eBC_{ff}	Apportioned eBC component from fossil fuel-based sources
BB(%)	Percentage of eBC_{bb} component from total eBC.

Section B: MA300 onboard correction method

The corrected eBC concentration is calculated by equation S1.

$$eBC_c = \frac{eBC_1}{(1 - k \times ATN_1)} \dots (S1)$$

Where, eBC_c is the compensated eBC concentration after the correction, k is the loading correction factor, ATN_1 refers the ATN values from channel 1 and eBC_1 refers to the non-corrected measurement corresponding to spot 1, given by MA300s. As identified by Drinovec (Drinovec et al., 2015), the above compensation equation (S1) is similar but not the same to Virkkula's equation (Virkkula et al., 2007). Moreover, Virkkula's (Virkkula et al., 2007) loading correction factor is calculated based on the data continuity from each filter spot. MA300 uses non-corrected eBC and ATN measurements from both the spots at each time stamp to estimate the compensation parameter and is given by equation S2.

$$k = \frac{BC_2 - BC_1}{(BC_2 \times ATN_1) - (BC_2 \times ATN_1)} \dots (S2)$$

It is important to note that MA300's data include both raw photometer readings and the compensated eBC concentrations for each wavelength channel, which provides opportunity to adapt AE33's algorithm and check for opportunities in improvement.

Section C: Data cleaning in MA300's raw data

We observed drifts in raw photometer sensor measurements from MA300s across the measurement period. These drifts can be attributed voltage fluctuation in the sensor readings in MA300. This is probably due to the use of lower quality (or lower cost) photometer in the MA300 as compared to the AE33. We consider these drifts outliers in the data collection. Based on inter quartile range (IQR) criteria, we have removed the drift points and results are shown in figure below (before and after removing outliers). The IQR criterion means that all observations above q0.75 + 1.5IQR or below q0.25 − 1.5IQR (where q0.25 and q0.75 correspond to first and third quartile respectively, and IQR is the difference between the third and first quartile) are considered as potential outliers by R programming software.

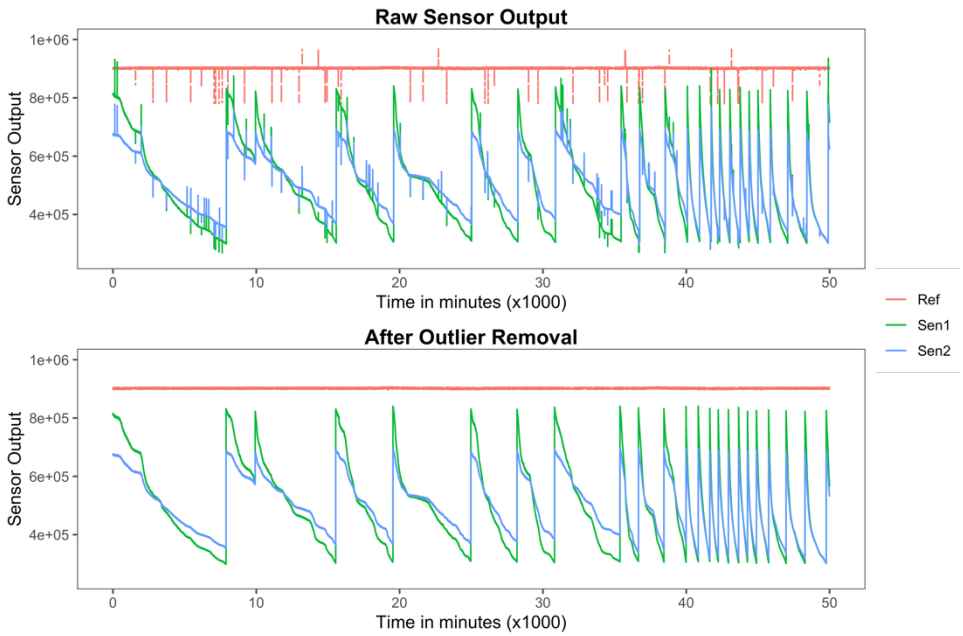

Figure S 1:Sample sensor readings (left panel with drifts, right panel after noise removal) from MA300 in Reference spot (Ref), Spot 1 (Sen1) and Spot 2 (Sen2).

Section D: Aethalometer model for eBC source apportionment

Aethalometer models have been developed by utilizing the power law relationship of aerosol light absorption (Main text, equation 6). The two-component model assumes light absorption is contributed by the two potential sources (eg. biomass burning and fossil fuel emission), which has been widely considered in estimating BC emission (Sandradewi et al., 2008; Rajesh and Ramachandran, 2017; Dumka et al., 2018; Healy et al., 2019). This model apportions the total spectral b_{abs} into $b_{abs,ff}$ (light absorption from fossil fuel emission) and $b_{abs,bb}$ (light absorption from biomass burning emission) and subsequently estimated the eBC_{bb} and eBC_{ff} concentrations. Equations S3 – S9, have been derived and used to estimating the source contributions at each timestamp of data collected. Here, α_{ff} and α_{bb} values are the largest source of uncertainty in the results (Healy et al., 2017; Zotter et al., 2017), which are typically derived from the 14C analysis of the aerosol samples. The values of α may also differ by location, aerosol composition and mixing state which can be constrained by additional measurements (Garg et al., 2016). In absence of additional measurements, α can be adopted from other but similar/representative studies (weather, source influence etc.). In this work, we utilized α values from two particular previous work: (1) performed at the similar site (Healy et al., 2019) and (2) recommend values from 14C based analysis (Zotter et al., 2017).

$$b_{abs}(\lambda) = b_{abs,ff}(\lambda) + b_{abs,bb}(\lambda) \quad \dots (S3)$$

$$\frac{b_{abs,ff}(\lambda_1)}{b_{abs,ff}(\lambda_2)} = \left(\frac{\lambda_1}{\lambda_2}\right)^{-\alpha_{ff}} \dots (S4)$$

$$\frac{b_{abs,bb}(\lambda_1)}{b_{abs,bb}(\lambda_2)} = \left(\frac{\lambda_1}{\lambda_2}\right)^{-\alpha_{bb}} \dots (S5)$$

$$b_{abs,bb} = \frac{b_{abs}(\lambda_1) - b_{abs}(\lambda_2) \times \left(\frac{\lambda_1}{\lambda_2}\right)^{-\alpha_{ff}}}{\left(\frac{\lambda_1}{\lambda_2}\right)^{-\alpha_{bb}} - \left(\frac{\lambda_1}{\lambda_2}\right)^{-\alpha_{ff}}} \dots (S6)$$

$$b_{abs,ff} = \frac{b_{abs}(\lambda_1) - b_{abs}(\lambda_2) \times \left(\frac{\lambda_1}{\lambda_2}\right)^{-\alpha_{bb}}}{\left(\frac{\lambda_1}{\lambda_2}\right)^{-\alpha_{ff}} - \left(\frac{\lambda_1}{\lambda_2}\right)^{-\alpha_{bb}}} \dots (S7)$$

$$eBC_{ff} = eBC \times \frac{b_{abs,ff}(\lambda)}{b_{abs}(\lambda)} \dots (S8)$$

$$eBC_{bb} = eBC \times \frac{b_{abs,bb}(\lambda)}{b_{abs}(\lambda)} \dots (S9)$$

Section E: Statistical comparison metrics

Systematic, quantitative performance analysis of MA300 derived quantities were done by utilizing different statistical metrics. To assess the consistency of MA300 reported data, we compared the results of MA300 units with the reference AE33 measurements and used single value performance metrics. We compare AE33's eBC concentration, multi-wavelength $b_{abs,\lambda}$ with MA300 instrument reported data. The parameters that were used in this study include: slope (b), coefficient of determination (R^2) and weighted R^2 (bR2) from the linear regression fit (with zero intercept), mean absolute `error (MAE), root mean squared error (RMSE), normalized root mean squared error (NRMSE). These parameters were selected based on previous studies which are focused on instrumental performance (Zimmerman, 2022; Malings et al., 2019), comparison studies (Alas et al., 2020; Rajesh and Ramachandran, 2018), or model evaluation (Zambrano-Bigiarini, 2020; Yao et al., 2013; Krstic et al., 2016). The equations which are used to calculate the parameters are given as follows:

$$MAE = \frac{1}{n}\sum|P_{AE33} - P_{MA300}|$$

$$RMSE = \sqrt{\frac{\sum_1^n (P_{AE33} - P_{MA300})^2}{n}}$$

$$NRMSE = \frac{RMSE}{\overline{P_{AE33}}}$$

$$bR2 = \begin{cases} |b| \times R^2, & for\ b \leq 1 \\ |b|^{-1} \times R^2, & for\ b > 1 \end{cases}$$

*P_{AE33} and P_{MA300} represents parameter (eg. eBC) from AE33 and MA300 respectively, $\overline{P_{AE33}}$ is the average concentration measured by AE33.

In this study, we primarily use linear fit parameters and MAE and NRMSE to assess the MA300's performance in different context. However, all the parameters mentioned above are estimated and provided in Table S4 and S5.

Table S1: Wavelength of light absorption measurement and corresponding Mass Absorption Cross section (MAC) for AE33 and MA300 considered in this study

Channel	*AE33*		*MA300*	
	Wavelength (nm)	*MAC (m^2/g)*	*Wavelength (nm)*	*MAC (m^2/g)*
1	370	18.47	375	24.069
2	470	14.54	470	19.07
3	520	13.14	528	17.028
4	590	11.58	625	14.091
5	660	10.35	880	10.12
6	880	7.77	--	--
7	950	7.19	--	--

Table S2: MA300 and AE33: Instrumental comparison and operational details

	AE33	**MA300**
Weight	20 kg (approx.)	0.715 kg
Power Requirement	AC (25 W typical)	AC + Battery Operated (46.08Wh)
Instrument Type	Dual Spot Aethalometer	Dual-Spot Micro-Aethalometer
Filter type	Teflon	PTFE
Sampling Spot Area	0.785 cm2	0.283 cm2
Wavelengths of Light Absorption (nm)	370, 470, 520, 590, 660, 880, 950	375, 470, 528, 625, 880
Filter Loading Correction	Using Drinovec 2015	Using Virkkula 2007
Scattering Correction	Using Drinovec 2015	Not Considered
Operational Details		
Flow Rate	5000 ml per minute	150 ml per minute
ATN range	0-120	0-100
Data Collection	1 min	1 min

Table S3 (a). Table of statistical parameters for the MA300 units vs AE33 : eBC

Period	eBC	MAE (µg/m³)	RMSE (µg/m³)	NRMSE (%)	bR2
Reg	MA300A	0.43	0.63	47.49	0.56
	MA300B	0.45	0.68	51.04	0.48
	MA300C	0.45	0.67	50.50	0.67
WF	MA300A	0.88	1.15	26.20	0.63
	MA300B	1.19	1.55	35.38	0.49
	MA300C	0.86	1.17	26.62	0.69

Table S3 (b). Table of statistical parameters for the MA300 units vs AE33 : b_{abs}

Period	b_{abs}	Channel	MAE (Mm^{-1})	RMSE (Mm^{-1})	NRMSE (%)	bR2
Reg	MA300A	UV	9.55	15.18	51.80	0.66
		Blue	7.69	11.84	52.73	0.64
		Green	6.67	10.08	52.39	0.65
		Red	5.83	8.71	61.47	0.58
		IR	3.92	5.87	56.53	0.62
	MA300B	UV	8.95	13.43	46.13	0.59
		Blue	7.03	10.66	47.55	0.58
		Green	6.02	9.00	46.89	0.59
		Red	4.75	7.02	49.55	0.65
		IR	3.41	5.02	48.40	0.64
	MA300C	UV	13.20	19.75	67.61	0.56
		Blue	10.79	16.11	71.75	0.53
		Green	9.25	13.83	71.92	0.53
		Red	8.33	12.28	86.56	0.48
		IR	5.46	8.05	77.63	0.52
WF	MA300A	UV	35.68	46.12	30.41	0.66
		Blue	19.55	26.13	30.10	0.67
		Green	16.10	21.03	30.32	0.66
		Red	16.08	20.00	41.39	0.58
		IR	9.60	12.11	35.59	0.60
	MA300B	UV	39.99	51.19	33.75	0.58
		Blue	18.40	23.96	27.60	0.64
		Green	14.30	18.81	27.12	0.63
		Red	10.07	13.48	27.90	0.68
		IR	7.02	9.40	27.63	0.64
	MA300C	UV	37.01	48.47	31.96	0.62
		Blue	23.46	31.06	35.78	0.61
		Green	19.44	25.52	36.80	0.59
		Red	19.97	24.68	51.07	0.51
		IR	13.23	16.19	47.56	0.53

Table S3 (C). Table of statistical parameters for the MA300 units vs AE33 : b_{absD}

Period	b_{abs}	Channel	MAE (Mm^{-1})	RMSE (Mm^{-1})	NRMSE (%)	bR2
Reg	MA300A	UV	13.55	20.79	71.16	0.52
		Blue	10.55	15.85	70.56	0.52
		Green	9.04	13.48	70.06	0.53
		Red	8.04	11.81	83.23	0.48
		IR	5.20	7.78	74.97	0.51
	MA300B	UV	10.89	16.13	55.25	0.49
		Blue	8.42	12.68	56.46	0.52
		Green	7.24	10.83	56.30	0.56
		Red	6.11	9.09	64.14	0.55
		IR	4.28	6.24	60.10	0.58
	MA300C	UV	16.94	25.63	87.43	0.47
		Blue	13.37	19.81	88.23	0.47
		Green	11.40	16.91	87.94	0.47
		Red	10.31	15.13	106.60	0.42
		IR	6.82	9.96	96.09	0.45
WF	MA300A	UV	48.80	62.06	40.92	0.43
		Blue	26.63	34.78	40.06	0.59
		Green	24.56	31.71	45.72	0.56
		Red	23.76	29.46	60.96	0.50
		IR	13.12	16.18	47.53	0.54
	MA300B	UV	46.69	62.10	40.84	0.47
		Blue	23.18	31.82	36.59	0.64
		Green	18.14	24.41	35.13	0.63
		Red	15.76	20.84	43.12	0.56
		IR	9.52	12.19	35.82	0.61
	MA300C	UV	40.57	52.19	34.33	0.56
		Blue	24.52	31.60	36.40	0.60
		Green	22.85	29.26	42.19	0.53
		Red	23.72	29.33	60.69	0.46
		IR	17.64	21.17	62.20	0.46

Table S4: Results of the linear relationship of MA300s and AE33

		Reg		*WF*	
Parameter	***Device***	***Slope (error)***	***R^2***	***Slope (error)***	***R^2***
eBC	MA300A	1.03 ± 0.01	0.86	1.06 ± 0.02	0.95
	MA300B	1.19 ± 0.01	0.86	1.27 ± 0.02	0.94
	MA300C	0.85 ± 0.01	0.87	0.95 ± 0.02	0.94
$b_{abs,UV}$	MA300A	0.86 ± 0.01	0.86	1 ± 0.02	0.93
	MA300B	1.01 ± 0.01	0.87	1.16 ± 0.02	0.93
	MA300C	0.7 ± 0.01	0.87	0.99 ± 0.02	0.92
$b_{abs,Blue}$	MA300A	0.83 ± 0.01	0.86	0.87 ± 0.01	0.95
	MA300B	0.98 ± 0.01	0.86	1.05 ± 0.02	0.94
	MA300C	0.68 ± 0.01	0.87	0.82 ± 0.01	0.94
$b_{abs,Green}$	MA300A	0.83 ± 0.01	0.87	0.86 ± 0.01	0.95
	MA300B	0.98 ± 0.01	0.86	1.05 ± 0.02	0.94
	MA300C	0.68 ± 0.01	0.87	0.81 ± 0.01	0.94
$b_{abs,Red}$	MA300A	0.75 ± 0.01	0.87	0.76 ± 0.01	0.95
	MA300B	0.88 ± 0.01	0.86	0.94 ± 0.02	0.94
	MA300C	0.62 ± 0.01	0.87	0.71 ± 0.01	0.94
$b_{abs,IR}$	MA300A	0.79 ± 0.01	0.86	0.81 ± 0.01	0.95
	MA300B	0.91 ± 0.01	0.86	0.97 ± 0.02	0.94
	MA300C	0.66 ± 0.01	0.87	0.73 ± 0.01	0.94

Table S5: Mean ± standard deviation of eBC components estimated from diurnal distribution from AE33, MA300 and MA300 with modified Drinovec corrected data

Period	**Wavelength**	**AE33**		**MA300**		**MA300+Drinovec**	
		eBC_{bb}	**eBC_{ff}**	**eBC_{bb}**	**eBC_{ff}**	**eBC_{bb}**	**eBC_{ff}**
Reg	UV-IR	0.17±0.04	1.14±0.36	0.12±0.02	1.09±0.29	0.13±0.03	1.24±0.32
	Blue-IR	0.24±0.05	0.91±0.31	0.17±0.03	0.95±0.26	0.18±0.04	1.08±0.28
WF	UV-IR	1.90±0.32	1.99±0.79	1.07±0.25	2.66±0.64	0.87±0.27	3.61±0.80
	Blue-IR	1.46±0.23	1.73±0.64	0.98±0.21	2.24±0.55	1.17±0.25	2.6±0.67

Fig S2: Wildfire smoke impact on eBC concentration

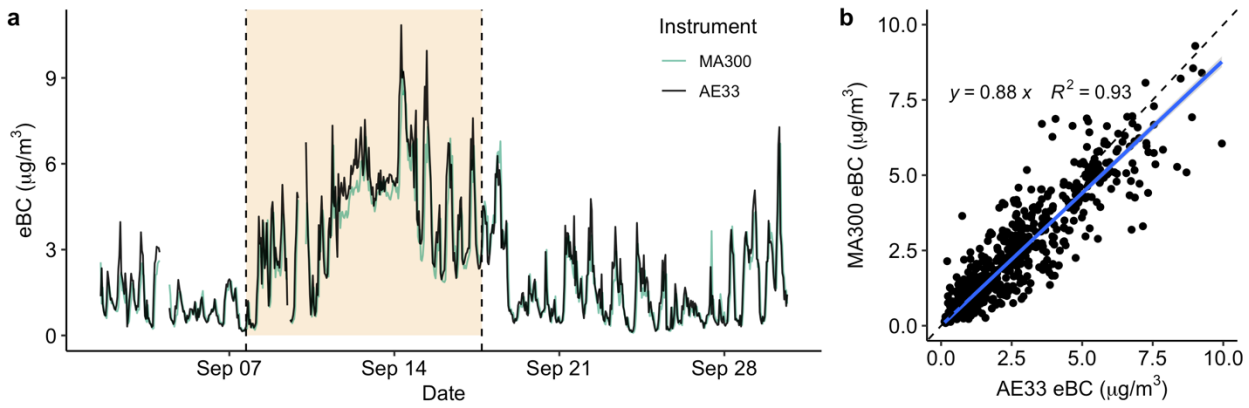

Figure S 2: Hourly eBC concentration measured by AE33 and mean of three MA300 units for September 2020 at Clark Drive. (a) Time series of the measurements with the yellow shaded region representing the wildfire smoke affected days (Sep 8 – Sep 18). (b) Scatter plot of the same data with liner fit (blue line). Dashed line represents the 1:1 line

Fig S3: Wavelength specific b_{abs} from AE33

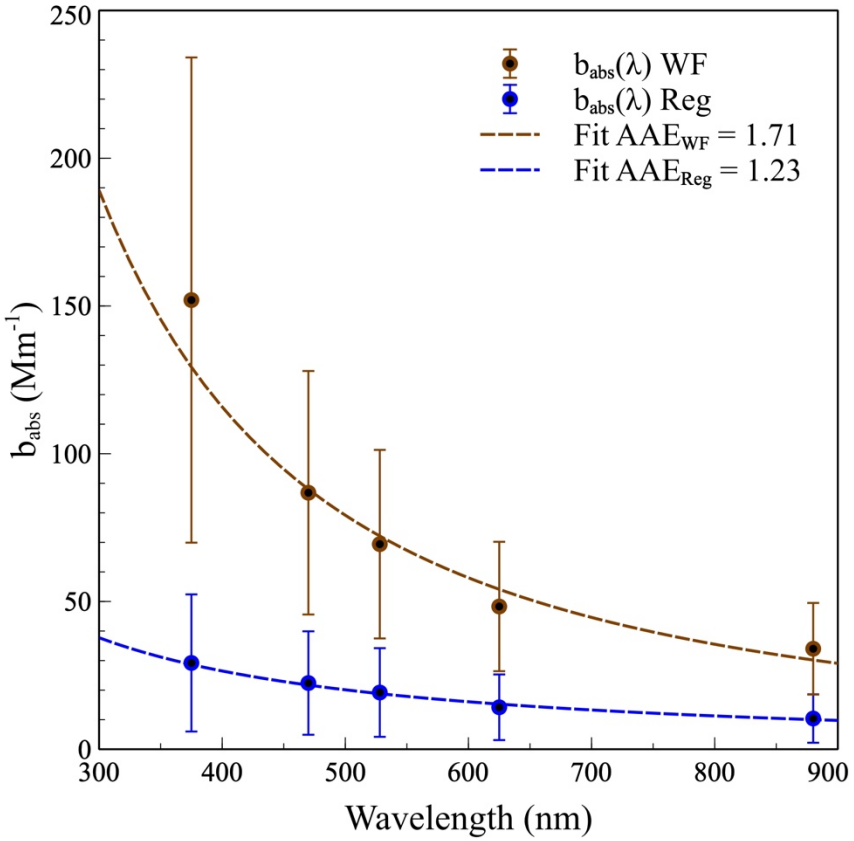

Figure S 3: Mean b_{abs} values measured during Reg and WF days by AE33 across five wavelengths. Error bar represents the standard deviation, and the dashed line represents the power law fit. AAE(exponent of the power law fit) has been mentioned for the two periods.

Fig S4: Wavelength specific b_{abs} from MA300

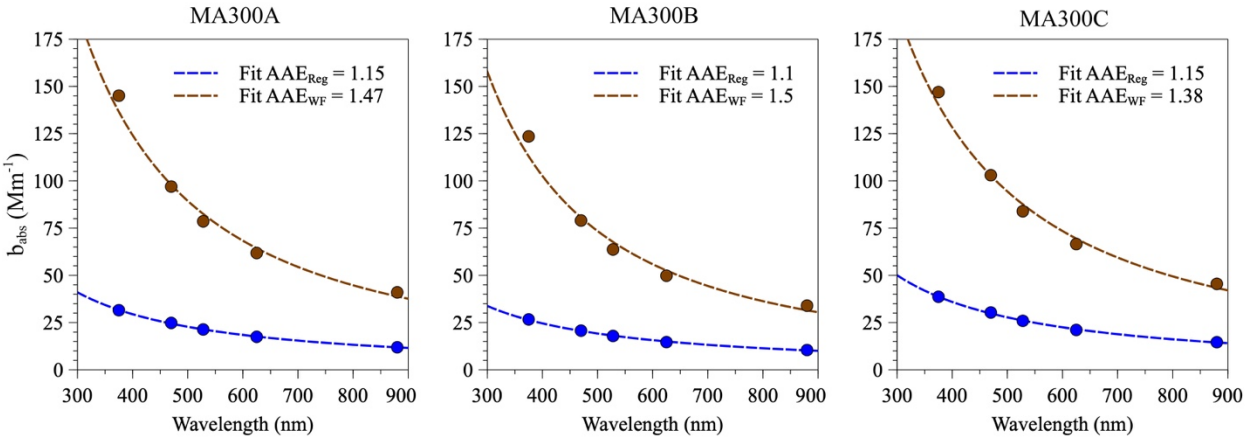

Figure S 4: Same as figure 7 but derived for MA300 units

Fig S5: Comparison of source apportionment results with wavelength pairs used

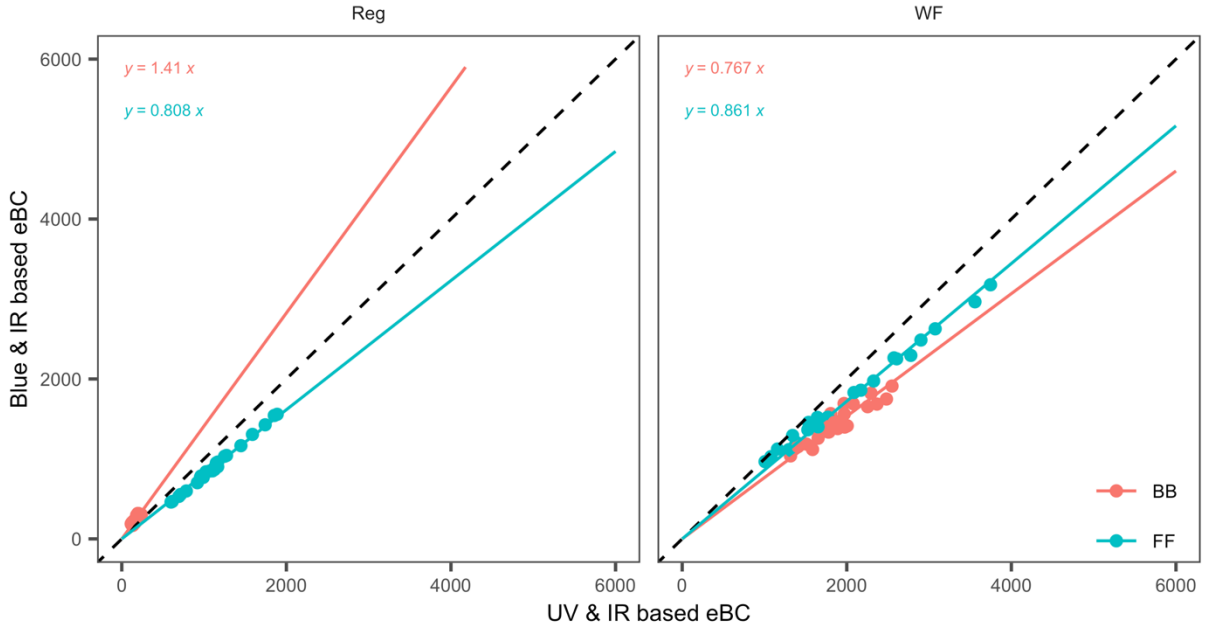

Figure S 5: Comparison of AE33 reported diurnal hourly eBC (ng/m3) contribution from eBC_{bb} and eBC_{ff} from UV-IR based and Blue-IR based source apportionment techniques

Fig S6: MA300 Source Apportionment Result from Onboard Correction

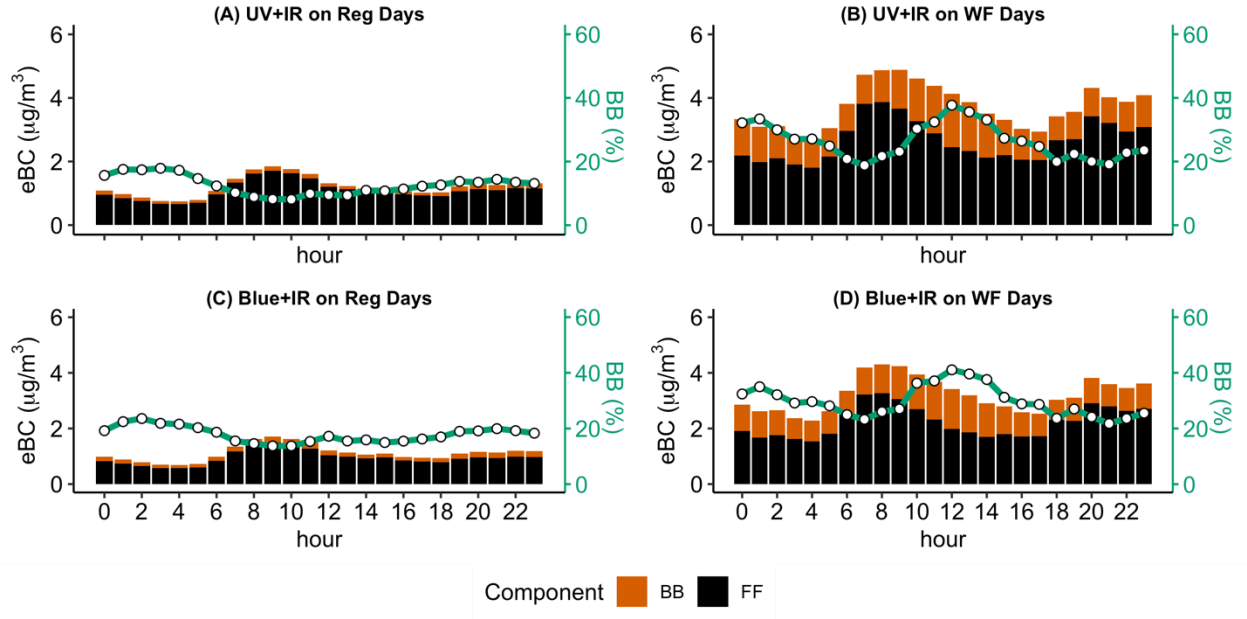

Figure S 6: Diurnal variation of eBC components (Similar to Figure 4 in main text) for MA300's onboard corrected data.

Fig S7: MA300 Source Apportionment Result from Modified Drinovec Correction

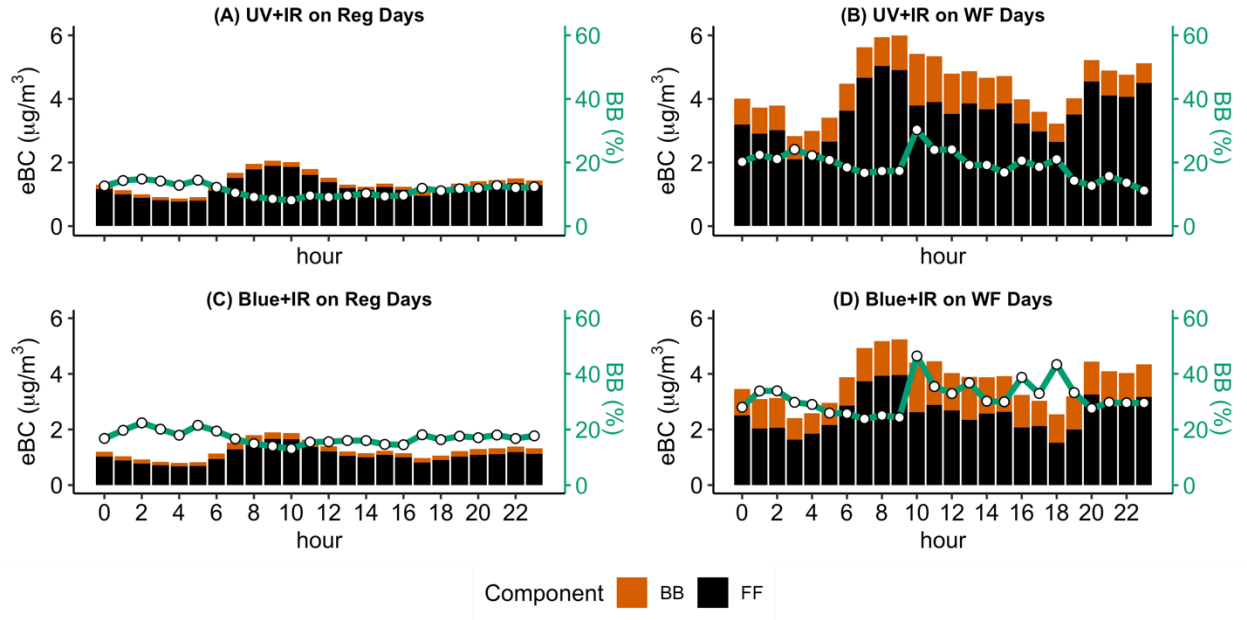

Figure S 7:Diurnal variation of eBC components (Similar to Figure 4 in main text) for modified Drinovec corrected data on MA300s raw measurement

Fig S8: Variability of eBC measurement by micro-aethalometer MA300

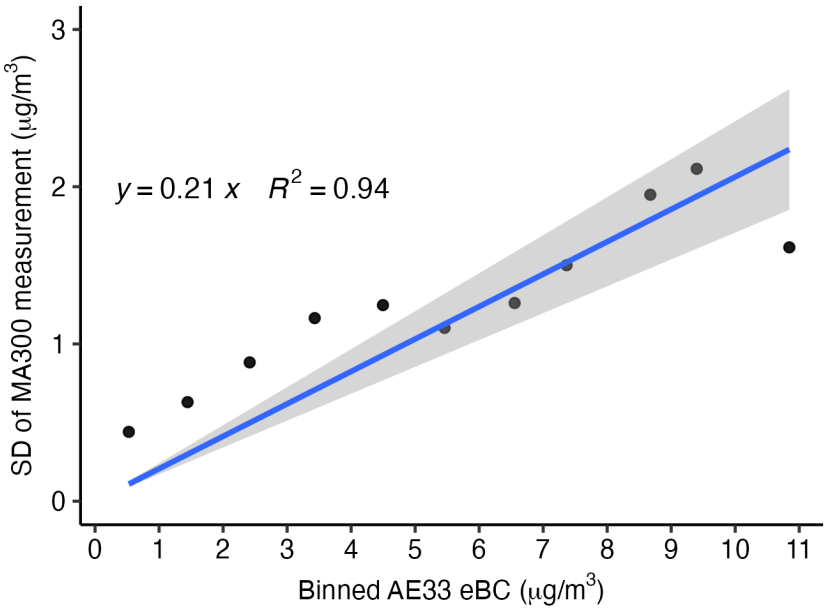

Figure S 8: Multi unit pooled standard deviation from MA300 measurements for each one μg/m³ of eBC concentration measured by AE33. The fit line (in blue) represents the linear response of MA300's variability across the concentration range. The shaded region represents the 95% CI of the fit.

Reference:

Alas, H. D. C., Müller, T., Weinhold, K., Pfeifer, S., Glojek, K., Gregorič, A., Močnik, G., Drinovec, L., Costabile, F., Ristorini, M., and Wiedensohler, A.: Performance of microAethalometers: Real-world Field Intercomparisons from Multiple Mobile Measurement Campaigns in Different Atmospheric Environments, Aerosol Air Qual. Res., 20, 2640–2653, https://doi.org/10.4209/aaqr.2020.03.0113, 2020.

Drinovec, L., Močnik, G., Zotter, P., Prévôt, A. S. H., Ruckstuhl, C., Coz, E., Rupakheti, M., Sciare, J., Müller, T., Wiedensohler, A., and Hansen, A. D. A.: The "dual-spot" Aethalometer: an improved measurement of aerosol black carbon with real-time loading compensation, Atmospheric Measurement Techniques, 8, 1965–1979, https://doi.org/10.5194/amt-8-1965-2015, 2015.

Dumka, U. C., Kaskaoutis, D. G., Tiwari, S., Safai, P. D., Attri, S. D., Soni, V. K., Singh, N., and Mihalopoulos, N.: Assessment of biomass burning and fossil fuel contribution to black carbon concentrations in Delhi during winter, Atmospheric Environment, 194, 93–109, https://doi.org/10.1016/j.atmosenv.2018.09.033, 2018.

Garg, S., Chandra, B. P., Sinha, V., Sarda-Esteve, R., Gros, V., and Sinha, B.: Limitation of the Use of the Absorption Angstrom Exponent for Source Apportionment of Equivalent Black Carbon: a Case Study from the North West Indo-Gangetic Plain, Environ. Sci. Technol., 50, 814–824, https://doi.org/10.1021/acs.est.5b03868, 2016.

Healy, R. M., Sofowote, U., Su, Y., Debosz, J., Noble, M., Jeong, C.-H., Wang, J. M., Hilker, N., Evans, G. J., Doerksen, G., Jones, K., and Munoz, A.: Ambient measurements and source apportionment of fossil fuel and biomass burning black carbon in Ontario, Atmospheric Environment, 161, 34–47, https://doi.org/10.1016/j.atmosenv.2017.04.034, 2017.

Healy, R. M., Wang, J. M., Sofowote, U., Su, Y., Debosz, J., Noble, M., Munoz, A., Jeong, C.-H., Hilker, N., Evans, G. J., and Doerksen, G.: Black carbon in the Lower Fraser Valley, British Columbia: Impact of 2017 wildfires on local air quality and aerosol optical properties, Atmospheric Environment, 217, 116976, https://doi.org/10.1016/j.atmosenv.2019.116976, 2019.

Krstic, G., Krstic, N., and Zambrano-Bigiarini, M.: The br2 – weighting Method for Estimating the Effects of Air Pollution on Population Health, Journal of Modern Applied Statistical Methods, 15, https://doi.org/10.22237/jmasm/1478004000, 2016.

Malings, C., Tanzer, R., Hauryliuk, A., Kumar, S. P. N., Zimmerman, N., Kara, L. B., Presto, A. A., and R. Subramanian: Development of a general calibration model and long-term performance evaluation of low-cost sensors for air pollutant gas monitoring, Atmos. Meas. Tech., 12, 903–920, https://doi.org/10.5194/amt-12-903-2019, 2019.

Rajesh, T. A. and Ramachandran, S.: Characteristics and source apportionment of black carbon aerosols over an urban site, Environ Sci Pollut Res, 24, 8411–8424, https://doi.org/10.1007/s11356-017-8453-3, 2017.

Rajesh, T. A. and Ramachandran, S.: Black carbon aerosol mass concentration, absorption and single scattering albedo from single and dual spot aethalometers: Radiative implications, Journal of Aerosol Science, 119, 77–90, https://doi.org/10.1016/j.jaerosci.2018.02.001, 2018.

Sandradewi, J., Prévôt, A. S. H., Szidat, S., Perron, N., Alfarra, M. R., Lanz, V. A., Weingartner, E., and Baltensperger, U. R. S.: Using aerosol light abosrption measurements for the quantitative determination of

wood burning and traffic emission contribution to particulate matter, Environmental Science and Technology, 42, 3316–3323, https://doi.org/10.1021/es702253m, 2008.

Virkkula, A., Mäkelä, T., Hillamo, R., Yli-Tuomi, T., Hirsikko, A., Hämeri, K., and Koponen, I. K.: A Simple Procedure for Correcting Loading Effects of Aethalometer Data, Journal of the Air & Waste Management Association, 57, 1214–1222, https://doi.org/10.3155/1047-3289.57.10.1214, 2007.

Yao, J., Brauer, M., and Henderson, S. B.: Evaluation of a Wildfire Smoke Forecasting System as a Tool for Public Health Protection, Environmental Health Perspectives, 121, 1142–1147, https://doi.org/10.1289/ehp.1306768, 2013.

Zambrano-Bigiarini, M.: Package 'hydroGOF,' Goodness-of-fit Functions for Comparison of Simulated and Observed, 2020.

Zimmerman, N.: Tutorial: Guidelines for implementing low-cost sensor networks for aerosol monitoring, Journal of Aerosol Science, 159, 105872, https://doi.org/10.1016/j.jaerosci.2021.105872, 2022.

Zotter, P., Herich, H., Gysel, M., El-Haddad, I., Zhang, Y., Močnik, G., Hüglin, C., Baltensperger, U., Szidat, S., and Prévôt, A. S. H.: Evaluation of the absorption Ångström exponents for traffic and wood burning in the Aethalometer-based source apportionment using radiocarbon measurements of ambient aerosol, Atmospheric Chemistry and Physics, 17, 4229–4249, https://doi.org/10.5194/acp-17-4229-2017, 2017.